

Contents lists available at [ScienceDirect](http://ScienceDirect.com)

Biochimica et Biophysica Acta

journal homepage: www.elsevier.com/locate/bbamem

A systematic molecular dynamics simulation study of temperature dependent bilayer structural properties

Xiaohong Zhuang^a, Judah R. Makover^a, Wonpil Im^{b,c}, Jeffery B. Klauda^{a,*}^a Department of Chemical and Biomolecular Engineering, University of Maryland, College Park, MD 20742, USA^b Department of Molecular Biosciences, The University of Kansas, Lawrence, KS 66047, USA^c Center for Bioinformatics, The University of Kansas, Lawrence, KS 66047, USA

ARTICLE INFO

Article history:

Received 19 March 2014

Received in revised form 7 June 2014

Accepted 11 June 2014

Available online 19 June 2014

Keywords:

Lipid bilayer

Molecular dynamics

Force field accuracy

Bilayer structure

ABSTRACT

Although lipid force fields (FFs) used in molecular dynamics (MD) simulations have proved to be accurate, there has not been a systematic study on their accuracy over a range of temperatures. Motivated by the X-ray and neutron scattering measurements of common phosphatidylcholine (PC) bilayers (Kučerka et al. *BBA*. 1808: 2761, 2011), the CHARMM36 (C36) FF accuracy is tested in this work with MD simulations of six common PC lipid bilayers over a wide range of temperatures. The calculated scattering form factors and deuterium order parameters from the C36 MD simulations agree well with the X-ray, neutron, and NMR experimental data. There is excellent agreement between MD simulations and experimental estimates for the surface area per lipid, bilayer thickness (D_B), hydrophobic thickness (D_C), and lipid volume (V_L). The only minor discrepancy between simulation and experiment is a measure of $(D_B - D_{HH}) / 2$ where D_{HH} is the distance between the maxima in the electron density profile along the bilayer normal. Additional MD simulations with pure water and heptane over a range of temperatures provide explanations of possible reasons causing the minor deviation. Overall, the C36 FF is accurate for use with liquid crystalline PC bilayers of varying chain types and over biologically relevant temperatures.

© 2014 Elsevier B.V. All rights reserved.

1. Introduction

Membrane lipids function as boundaries to cells and internal organelles and regulate the molecular traffic across the boundaries [1]. Together with sterols, phospholipids are the main structural components of membranes [1], and their studies are necessary to understand the role and mechanisms on how membrane lipids regulate molecular transport as well as protein function [2]. Phosphatidylcholine (PC) lipids (GP0101 according to the lipidomics classification [3]) are neutral zwitterionic glycerophospholipids in which two fatty acids are attached through a phosphodiester linkage to the third carbon with choline as its polar head group (Fig. 1). When amphipathic PC lipids are mixed with water at the correct water to lipid ratio, bilayers spontaneously form, in which the nonpolar acyl chains remain in the center and the outer polar head groups interact with the aqueous phase [1].

Cell membrane bilayers are usually in the liquid crystalline phase (L_α) [2]. As the temperature decreases below a certain melting temperature, a phase transition from L_α to the gel phase (L_β) occurs [4]. Even though the physiological temperature of the human body is nearly constant, microorganisms live in varying temperatures, which influences cell membrane properties, such as flexibility [5,6], cell adhesion [7], metabolism [8], permeability [8], and also membrane structure. The

variation of these properties is commonly related to the change in membrane fluidity. As the temperature increases, the membrane fluidity increases [7]. Many properties of pure phospholipid bilayers mimic the cell membranes effectively even though they do not provide all the complexities [9]. Thus, this model is often used to study various biomembrane topics when the biological membrane is too complex for experimentation [9].

Biomembrane functionalities strongly depend on their structures. Therefore, considerable efforts have been made to estimate the membrane structural parameters, such as surface area per lipid (SA/lipid), volume per lipid (V_L), hydrophobic thickness (D_C), overall bilayer thickness (D_B), and deuterium order parameters (S_{CD}). Atoms in the fluid bilayer phase are much more disordered than crystals, so that the traditional crystallographic analysis is not adequate to obtain the structural information [10]. However, small angle X-ray and neutron scattering (SAXS/SANS) can be applied to determine the lipid structural parameters, such as the overall bilayer thickness and molecular volume, from which the surface area and area compressibility modulus can be determined [10]. The partially dehydrated bilayer lipids (at a certain relative humidity) are not appropriate samples for the measurement because the lipid bilayers are distorted and structural properties are changed, but this issue can be avoided if fully hydrated liquid crystalline bilayers or unilamellar vesicles are used [11]. Unfortunately, significant discrepancies always exist between the SA/lipid of phospholipids determined by the X-ray and neutron scattering methods [12]. Instead of analyzing

* Corresponding author.

E-mail address: jbklauda@umd.edu (J.B. Klauda).

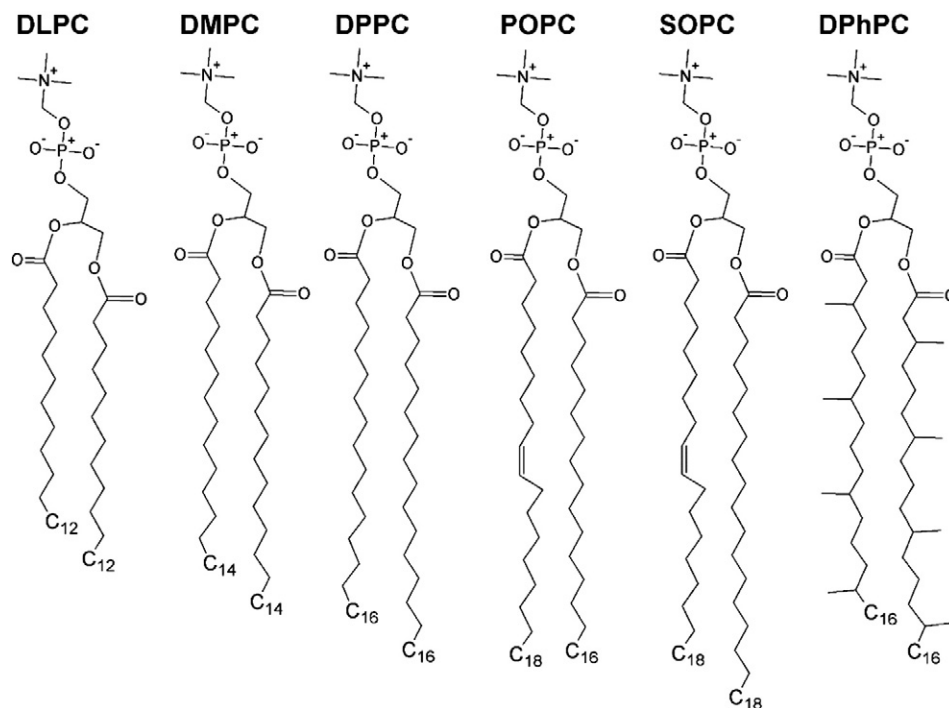


Fig. 1. Chemical structures of six phosphatidylcholine (PC) lipids simulated in this study: 1,2-dilauroyl-*sn*-glycero-3-PC (DLPC), 1,2-dimyristoyl-*sn*-glycero-3-PC (DMPC), 1,2-dipalmitoyl-*sn*-glycero-3-PC (DPPC), 1-palmitoyl-2-oleoyl-*sn*-glycero-3-PC (POPC), 1-stearoyl-2-oleoyl-*sn*-glycero-3-PC (SOPC), and 1,2-diphytanoyl-*sn*-glycero-3-PC (DPhPC).

the data separately, Kučerka et al. [13] proposed to simultaneously analyze both X-ray and neutron scattering data. By this method, experimental data on a few common PC lipid bilayers were measured to estimate their SA/lipid and thicknesses by fitting the scattering density profile (SDP) model [13] to the scattering data.

Due to the experimental constraints, molecular dynamics (MD) simulation is also extensively used to determine the lipid membrane structural properties. The all-atom CHARMM36 force field (C36 FF) developed by Klauda et al. [14] allows for accurate constant molecule number, pressure, and temperature (*NPT*) simulations of pure lipid bilayers. Moreover, it is capable of matching various structural and dynamical properties of lipid membranes, which results in more realistic membrane models, including lipid molecules containing branched chains [15]. MD simulations with the C36 FF have been used to study the lipid bilayers with cholesterol [16], membrane proteins [17], and micelles [18]. However, it has not been applied to examine the temperature dependent bilayer properties systematically. In this paper, to further verify the accuracy of the C36 FF, we provide MD simulation results of six common PC lipid bilayers (Fig. 1) over a wide range of temperatures and comparisons with experimental data obtained by Kučerka et al. [19]. We also calculated S_{CD} of the PC lipids from simulations and compared them to the experimental NMR S_{CD} values at varied temperatures. Overall, our results indicate that the C36 FF is accurate for use with liquid crystalline PC bilayers of varying chain types and over biologically relevant temperatures.

2. Methods

2.1. System setup and MD simulation protocol

Simulations were performed on six common PC lipids of varying lipid chains (Fig. 1). A set of three lipids that contain fully saturated (unbranched) chains were simulated with chain lengths of 12, 14, and 16: 1,2-dilauroyl-*sn*-glycero-3-PC (DLPC), 1,2-dimyristoyl-*sn*-glycero-3-PC (DMPC), 1,2-dipalmitoyl-*sn*-glycero-3-PC (DPPC). Two monounsaturated lipids on the *sn*-2 chain were studied: 1-palmitoyl-2-oleoyl-*sn*-glycero-3-PC (POPC) and 1-stearoyl-2-oleoyl-*sn*-glycero-3-PC (SOPC). A quad-

branched chain lipid, 1,2-diphytanoyl-*sn*-glycero-3-PC (DPhPC), was also simulated. Among all six lipids, POPC is the only lipid with unequal chain lengths between *sn*-1 and *sn*-2.

CHARMM-GUI *Membrane Builder* [20–22] was used to build these lipid membrane systems. Each bilayer system was built in a tetragonal box containing a total of 72 lipid molecules (36 per leaflet) and about 30 water molecules per lipid to make sure that lipids were fully hydrated without ions (Table 1). These simulations used the standard TIP3P water model [23,24] with the C36 lipid parameter set [14]. The van der Waals interactions were smoothly switched off between 8 and 12 Å by a forced-based switching function [25]. All the bond lengths involving hydrogen atoms were constrained using the RATTLE algorithm [26]. Particle mesh Ewald fast Fourier transform [27] was used for electrostatic interactions with an interpolation order of 6 and a direct space tolerance of 10^{-6} . The NAMD program [28] was used to equilibrate the lipid bilayer systems using the standard *Membrane Builder* six-step equilibration process [20,29] of gradually turning off restraints on the lipids over 200 ps at a temperature of 30 °C. The lipids were further thermally equilibrated for 750 ps without any restraints. For each lipid, the 30 °C equilibrated system was used to perform the production run at different target temperatures (Table 1). The temperature choices of the simulations depend on gel-transition temperatures of individual lipids (Table S1 in Supplementary material section). All simulations were run for 50–200 ns (Table 1) and equilibration was determined based on the SA/lipid. The simulation time-step was 2 fs, and the data was collected every 1 ps. All simulations were run in the *NPT* ensemble in tetragonal cell ($X = Y \neq Z$) with a pressure set to 1 bar. Langevin dynamics was used to maintain constant temperature for each system, while the Nosé-Hoover Langevin-piston algorithm [30,31] was used to maintain constant pressure. The Visual Molecular Dynamics (VMD) [32] program was used to create snapshots of the bilayers.

MD simulations were also performed on neat water and *n*-heptane to compare the temperature dependence of lipids with that of representative simple small molecules. Packmol [33] was used to build 300 water molecules and 80 heptane molecules. Cubic boxes were used for bulk water and *n*-heptane systems, which were both thermally equilibrated for 1 ns. The simulations were also run with NAMD with the

Table 1
Molecular dynamics simulation system information.

Lipid	# lipids	# waters	# atoms	# waters per lipid	Simulation temperatures (°C)	Simulation time (ns)
DLPC	72	2900	14,112	40.3	20, 30, 40, 50, 60	180, 70
DMPC	72	3071	14,976	42.7	30, 50, 60	50
DPPC	72	2364	15,840	32.8	50, 60	150
POPC	72	2476	16,128	34.4	10, 20, 30, 40, 50, 60	200, 100
SOPC	72	2540	16,560	34.0	10, 20, 30, 40, 50, 60	200, 100
DPhPC	72	2953	17,568	41.0	20, 30, 40, 50, 60	160, 100

same simulation protocols as for the PC lipid systems. The production runs for both water and heptane were simulated for 100 ns at temperatures ranging from 20 to 60 °C.

2.2. Analysis

The exact time with which the membrane systems are considered to be at equilibrium differs for different systems, depending on the convergence of the SA/lipid. Even for the same lipid, as the temperature varies, the system may reach equilibrium at different simulation times. All MD simulations were equilibrated by 50 ns. Therefore, the averages of all calculated properties were taken from 50 ns to the end of the simulation (except DMPC for which we used 26–50 ns). Block averages were used to obtain the statistical errors. The SA/lipid was based on the area of the simulation box divided by the number of lipids per leaflet.

While the SA/lipid provides information in the lateral lipid density, the electron density profiles (EDPs) can give information on how the density changes along the membrane normal. Calculating EDPs of every lipid atom is computationally demanding (required for comparison with scattering data); therefore, only the last 20–30 ns were used for the calculation using the CHARMM program [34]. The SIMtoEXP program [35] was used to convert the EDPs to form factors ($|F(q)|$) by combining the atomic electron densities and including their individual q dependence where q is the total scattering vector. For the trajectory analysis (EDPs, form factors, and volume probabilities), each atomic electron density (calculated by CHARMM) was combined into the following groups: choline, phosphate, glycerol, carboxyl, methylene (CH_2), methine (CH) (if there is any double bond), methyl (CH_3), and water [36]. This grouping differs slightly from that used by Kučerka et al. (the SDP structural model) to fit experimental scattering data in order to obtain the SA/lipid and other structural properties (see below) [19]. However, for our simulation data, no structural model is required, since we are able to calculate the SA/lipid directly.

Unlike other structural parameters, robust values of the lipid headgroup-to-headgroup distance (D_{HH}) and the overall bilayer thickness (D_{B}) can be directly estimated from scattering data without any structural model. D_{HH} can be obtained by measuring the distance between the peaks in the EDPs which are best resolved from X-ray scattering. Neutron scattering provides a high contrast between protonated lipid and deuterated water, from which D_{B} can be obtained [19]. However, as mentioned above, Kučerka et al.'s interpretation of scattering data requires a structural model to find more accurate D_{B} , D_{HH} , and hydrophobic thickness (D_{C}), from which the SA/lipid is obtained.

For MD simulations, D_{HH} is still defined as the distance between the peaks in the EDPs, however, D_{B} is defined as the distance between the midpoints of water based on their volume probabilities; D_{C} is defined as a half of the distance between the midpoints of bilayer's hydrocarbon acyl chains based on their volume probabilities [19]. There are more uncertainties involved in determining D_{HH} than D_{B} and D_{C} since the plateau may exist near the maximum EDPs instead of sharp peaks.

Experimentally, lipid volume V_{L} is measured, the thicknesses are obtained from a (SDP) model fit to both X-ray and neutron scattering data, and then the SA/lipid (or A in Eq. (1)) and other structural parameters can be estimated. However, in MD simulation studies, the SA/lipid can be directly obtained, and V_{L} can be calculated based on the following relation [11],

$$V_{\text{L}} = \frac{1}{\rho_{\text{w}}} (n_{\text{L}} - 0.5AF(0)) \quad (1)$$

where n_{L} is the number of electrons of lipid, A is the SA/lipid, $F(0)$ is the X-ray scattering form factor values at $q = 0$, and ρ_{w} is the electron density of water. The values of ρ_{w} and $F(0)$ are obtained from analysis of the EDPs in SIMtoEXP.

The slope (thermal coefficient) and its standard error for the area and thicknesses were calculated by a linear regression. The propagation of error method was used to obtain the standard errors of the area thermal expansivity ($\alpha_{\text{A}} = (\partial A/\partial T)/A$) and the thickness contractivities ($\alpha_{\text{DB}} = -(\partial D_{\text{B}}/\partial T)/D_{\text{B}}$ and $\alpha_{\text{DC}} = -(\partial D_{\text{C}}/\partial T)/D_{\text{C}}$) [19].

A final measure of lipid structure compared in this study is the deuterium order parameter (S_{CD}), which is experimentally measured by nuclear magnetic resonance (NMR). It can also be calculated from our simulation data by the following equation [37,38]:

$$S_{\text{CD}}^{(i)} = \left\langle \left| \frac{3}{2} \cos^2 \theta_i - \frac{1}{2} \right| \right\rangle \quad (2)$$

where θ_i is the angle between the CH-bond on the i th carbon and the bilayer normal and the angular bracket denotes a time and ensemble average.

3. Results and discussion

Some example snapshots at the end of the MD simulations are shown in Fig. 2. The results presented in the following subsections are ordered as: 1. comparison of MD-based form factors and experimental X-ray/neutron form factors (XFF/NFF) [19], which is the most reliable and direct comparison among all analyses; 2. comparison of MD-based data to experimentally estimated SA/lipid, D_{B} and D_{C} [19], and V_{L} [11, 13, 39, 40], and also the discussion about the temperature dependence of each structural parameter; 3. analyses of the EDPs resulted from simulations; 4. comparison of MD-based S_{CD} to NMR S_{CD} [41, 42]; 5. qualitative comparison of estimated $\Delta D_{\text{B-HH}}$ (i.e., $(D_{\text{B}} - D_{\text{HH}}) / 2$) to the experimental data [11, 13, 19, 39, 40, 43, 44]; 6. comparison of the simulated densities to experimental values of neat water [45] and heptane [46] at varied temperatures to elucidate minor deviation in scattering form factors and discrepancies in structural parameters between simulations and experiments.

3.1. Form factors $|F(q)|$

Experimental XFF and NFF are obtained from the measured scattering intensities. MD-based form factors are obtained by Fourier transformation of the electron/neutron density data considering the q dependence of atomic scattering functions via the SIMtoEXP program [35]. MD-based form factors provide a direct comparison with experimental data without any model assumption and fits [19]. Therefore, compared to other metrics obtained from scattering experiments, form factor comparison is the most persuasive method to test the accuracy of force fields [36]. XFFs of all the lipids in H_2O are obtained from reference [19]. For certain temperatures, experimental form factors of oriented bilayer stacks are provided in addition to the extruded unilamellar vesicles (ULVs) with a diameter of ~ 600 Å [47]. As shown in Fig. 3b, the XFF from ULV shows high resolution in the first two lobes, while the oriented sample results in high resolution in the second

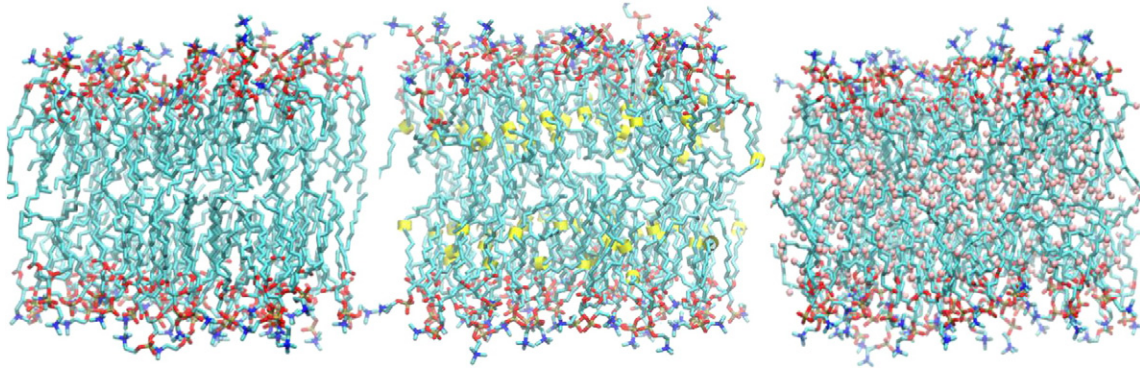


Fig. 2. Lipid bilayer system snapshots at the end of the simulations: DMPC at 30 °C, 50 ns (left), SOPC at 50 °C, 100 ns (middle), and DPhPC at 30 °C, 160 ns (right). The traditional color scheme is applied: cyan for carbon, blue for nitrogen, red for oxygen, and orange for phosphate. Yellow represents the double bond in SOPC and pink is for branch and terminal methyl groups in DPhPC. The hydrogen atoms and water molecules are not shown for clarity.

and third lobes; these two sets of data overlap well in the second lobe, so the structural difference caused by curvature stress is considered negligible [11]. Moreover, the undulation correction was made to the oriented bilayer sample to avoid the differences of structural parameters caused by the fluctuation of bilayers [11].

Fig. 3 shows that the MD-based form factors of POPC generally match well with the experimental XFF in the first lobe. However, for the second lobe, the MD-based form factors shift slightly to the left and have a higher peak compared to experiments. Moreover, although the MD-based and experimental form factors agree well at 30 °C, minor discrepancy appears in the higher temperatures (see Supplementary Figs. S1–5 for other lipid types). The degree of deviation increases as the temperature increases, indicating the different temperature dependence of the MD-based and experimental electron densities. These behaviors are also observed in DLPC (Fig. S1), DMPC (Fig. S2), and SOPC (Fig. S4). The form factors agree well for DPPC at 50 °C (Fig. S3), while the most deviation in the first lobe among all lipids is observed in DPPC at 60 °C. In the case of DPhPC (Fig. S5), however, the MD-based and experimental XFF match very well in all three lobes and all temperatures.

According to Kučerka et al. [11], for the first lobe in the small q range, the overall scattering intensity is much greater than that of the background water signal, meaning that the electron density of water barely

affects the first lobe. Therefore, the difference between the MD-based and experimental XFF for the first lobe is caused by deviation of lipid properties only. However, for the second lobe, the overall scattering intensity is close to the water intensity, meaning that the form factors strongly depend on the electron density of water. This implies that the deviation in the second lobe may be caused by inaccuracies in either the lipid or water density. For all lipids, the MD-based and experimental data of all the crossing points (i.e., $F(q) = 0$) match well, indicating that the thicknesses are in good agreement [11]. However, except for DPhPC, the minor differences exist in the second lobe for other lipid types at temperatures besides 30 °C. Since TIP3P deviates from the experimental density at these temperatures (see below), the electron density of water in the simulation is likely the cause for this (minor) second lobe discrepancy.

Through performing the SANS experiment [19], NFFs were determined at three different contrast conditions (i.e., 100%, 70%, and 50% D_2O). Fig. 4a–e shows that the higher deuterium concentration obviously results in higher NFFs, as expected. For $q < 0.2$, the MD-based NFF matches the experimental NFF very well, and this is the case for all lipids (Figs. S6–10). Based on this result, we expect that MD-based D_B should be very close to the robust D_B value estimated from neutron scattering. The deviations in XFFs demonstrate the possible deviation of MD-based and experimentally estimated D_{HH} .

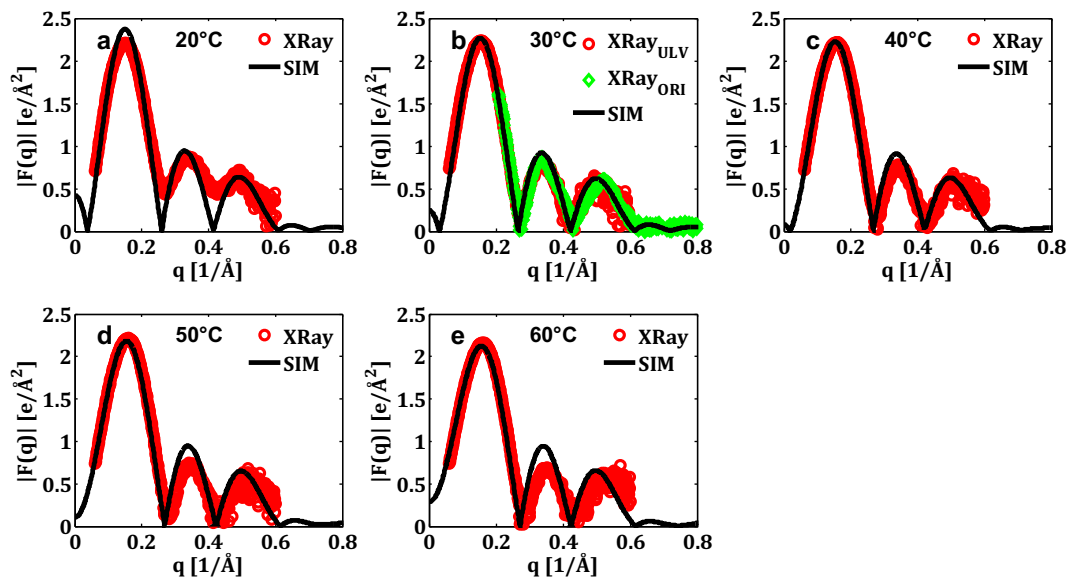


Fig. 3. Comparison of MD-based form factor data (the black curve) to X-ray experimental form factor of POPC (from ULV in red and from oriented bilayers in green) [19].

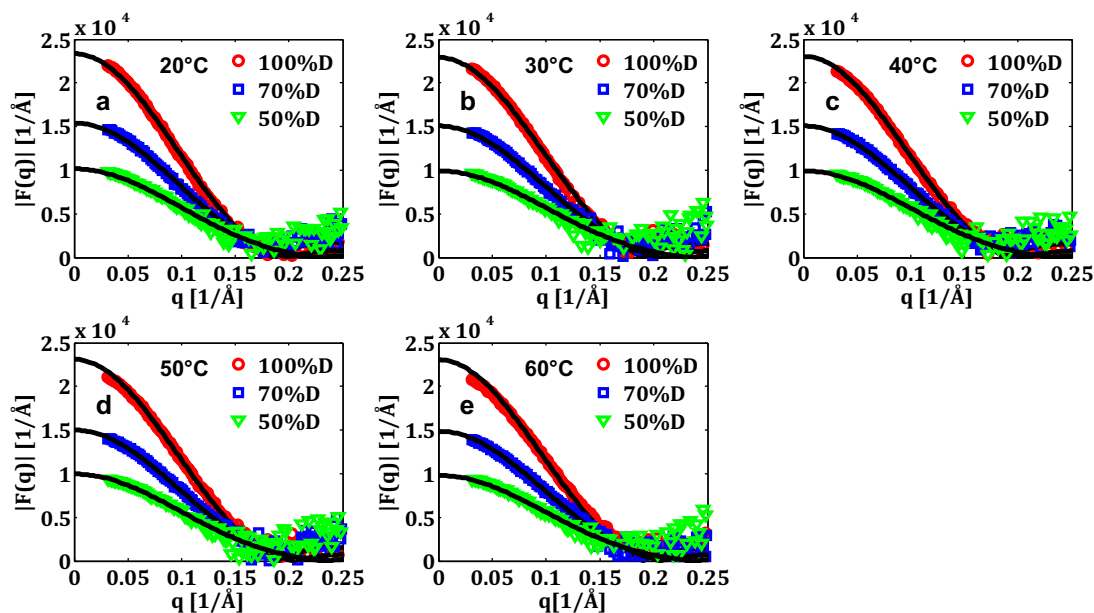


Fig. 4. Comparison of MD-based form factor to deuterium neutron scattering experimental data of POPC [19] in three contrasts. %D is %D₂O. The black curves are the MD-based form factor at each corresponded deuterium concentration.

3.2. Surface area, bilayer thicknesses, and molecular volume

The model-free C36 MD-based SA/lipid and bilayer and hydrophobic thicknesses (D_B and D_C) are compared to Kučerka et al.'s experimentally estimated data [19] based on the SDP model [13]. Overall, the C36 MD simulation data result in good agreement with the experimental SA/lipid (Table 2), D_B (Table 3), and D_C (Table 4), which are also plotted in Fig. 5. At the same temperature, the SA/lipid of POPC and SOPC are larger than the saturated DLPC, DMPC, and DPPC, because the *cis* double bond produces a permanent kink in the hydrocarbon chains that force the chain to occupy more cross-sectional area [9]. Though DPhPC has the same backbone hydrocarbon chain length as DPPC (16:0/16:0), the SA/lipid of the branched DPhPC is much greater at the same temperature. For DMPC (Fig. 5b), the SA/lipid, D_B , and D_C from the C36 simulations are almost superimposed on the experimental values at all temperatures. The SA/lipid of DPPC, SOPC, and DPhPC are underestimated at all temperatures. The MD-based D_B and D_C tend to agree better with experiment at the higher temperature of 60 °C, but are underestimated at lower temperatures. The simulated D_{HH} data are shown in Table S2, which are excluded in our major discussions as there are very few available experimental D_{HH} values to support the analysis.

Table 2
Surface area (SA) per lipid (Å²) at different temperatures.

Lipid	20 °C	30 °C	50 °C	60 °C
DLPC	62.3 ± 0.3 (59.6 ± 1.2)	63.1 ± 0.3 (60.8 ± 1.2)	64.3 ± 0.3 (64.8 ± 1.3)	66.0 ± 0.2 (65.9 ± 1.3)
DMPC	Gel	60.2 ± 0.6 (59.9 ± 1.2)	63.1 ± 0.3 (63.3 ± 1.3)	65.0 ± 0.4 (65.7 ± 1.3)
DPPC	Gel	Gel	61.8 ± 0.3 (63.1 ± 1.3)	63.4 ± 0.4 (65.0 ± 1.3)
POPC	63.7 ± 0.3 (62.7 ± 1.3)	65.5 ± 0.3 (64.3 ± 1.3)	67.8 ± 0.3 (67.3 ± 1.3)	68.7 ± 0.3 (68.1 ± 1.4)
SOPC	62.9 ± 0.3 (63.8 ± 1.3)	65.2 ± 0.3 (65.5 ± 1.3)	65.9 ± 0.2 (68.1 ± 1.4)	68.0 ± 0.2 (69.4 ± 1.4)
DPhPC	77.5 ± 0.2 (78.0 ± 1.6)	79.3 ± 0.1 (80.6 ± 1.6)	81.4 ± 0.2 (83.6 ± 1.7)	83.0 ± 0.2 (84.8 ± 1.7)

The data in the first row are MD-based values with standard errors, and in the second rows with parentheses are the experimentally-estimated values with uncertainties obtained by Kučerka et al. [19].

A distinct temperature effect is observed for these structural parameters (Tables 2–4, S2, and Fig. 5). Consistent with thermal expansion, as the temperature increases, the SA/lipid increases. Except for D_B of DPhPC, the thickness decreases as the temperature increases. The MD-based SA/lipid slope, k_A , is either equal to or slightly smaller than experimental values (Table S3). The MD-based thickness slopes, k_{DB} and k_{DC} , have a smaller magnitude than experiment (Tables S4–5), indicating that the temperature effect is relatively weaker for the C36 simulations but are all negative in agreement with experiment (except for k_{DB} of DPhPC). All the k_A are much larger than k_D in terms of its magnitude, which indicates stronger temperature dependence of the SA/lipid than the thicknesses. The absolute values of slopes k_A , k_{DB} , and k_{DC} of POPC and SOPC are smaller than those of DMPC and DPPC, implying that the temperature dependence of the SA/lipid and thicknesses of monounsaturated PC lipids are weaker than saturated lipids.

Compared to other lipids, DPhPC bilayers show slightly different temperature dependence. Both D_B and D_C of DPhPC from simulations show very weak temperature dependence. This is consistent with experiment as the slopes are close to zero and the k_{DC} can be either positive or negative statistically (Table S5). Unlike the experimental k_A of DPhPC, which is between monounsaturated and saturated lipids, the MD-based k_A of DPhPC is similar to the monounsaturated PC lipids. Consistent with experiments, the simulated DPhPC has smaller k_A , k_{DB} , and k_{DC} than DPPC, indicating that branched PC lipids have weaker temperature dependence than lipids with linear acyl hydrocarbon chains.

Besides the SA/lipid and thicknesses, the MD-based volume per lipid (V_L) was calculated based on Eq. (1). Fig. 6a and Table S6 summarize the comparison between MD-based and experimental V_L [11,13,40,48]. The MD-based V_L of DPPC, POPC, and SOPC show excellent agreement with experimental data, while the simulated V_L of DLPC and DMPC are overestimated, and DPhPC shows a slightly lower value than experimental V_L . The slopes k_{V_L} of the saturated lipids range from 0.91 (for DLPC) to 1.59 (for DPPC), showing that the temperature effect of V_L is stronger for lipids with longer acyl chains. Additionally, unlike model-dependent experimentally estimated SA/lipid and thicknesses, the V_L of PC lipids are measured more accurately [19] by the experimental method [48–50]. Therefore, V_L comparisons provide better experimental evidence than the SA/lipid and thicknesses.

The discrepancy between simulated and experimental SA/lipid, D_B , and D_C as well as their slopes may be due to minor C36 and TIP3P FF

Table 3
Overall bilayer thickness (D_B) of lipids (Å) at different temperatures.

Lipid	20 °C	30 °C	50 °C	60 °C
DLPC	30.9 (33.0 ± 0.7)	31 (32.6 ± 0.7)	31.1 (31.0 ± 0.6)	30.4 (30.7 ± 0.6)
DMPC	Gel	36.2 (36.7 ± 0.7)	35.3 (35.2 ± 0.7)	34.3 (34.2 ± 0.7)
DPPC	Gel	Gel	39.6 (39.0 ± 0.8)	38.9 (38.1 ± 0.8)
POPC	38.3 (39.8 ± 0.8)	37.4 (39.1 ± 0.78)	37.3 (37.9 ± 0.8)	37.0 (37.7 ± 0.8)
SOPC	40.9 (40.8 ± 0.8)	39.6 (40.0 ± 0.8)	40 (39.0 ± 0.8)	38.9 (38.5 ± 0.8)
DPhPC	33.5 (36.3 ± 0.7)	34.1 (35.4 ± 0.7)	34.1 (34.7 ± 0.7)	33.7 (35.2 ± 0.7)

The data in the first row are MD-based values, and in the second row with parentheses are the experimental values with uncertainties obtained by Kučerka et al. [19].

inaccuracies or, as mentioned above, due to the inaccuracy of the SDP model used to fit XFF and NFF to obtain these experimental values. It is possible as we and others have shown that multiple solutions to the SDP model parameters can provide decent fits to the form factor data [51–53]. This is also supported by the fact that MD-based form factors match NFF excellently (Fig. 4), but there are some minor discrepancies in MD-based and SDP model-based experimental D_B . Therefore, the overall agreement between experiment and MD simulations with the C36 FF is excellent considering these limitations in interpretation of experimental data.

3.3. Electron density profiles (EDPs)

The EDP is calculated by averaging the electron density over the course of the data collection period (see the Methods section). Since our lipid bilayer systems are symmetric and centered at $z = 0$, an additional averaging is used for positive and negative z EDP. The $z = 0$ point contains the terminal methyl groups of the hydrocarbon chains and has the lowest total electron density. As shown in Fig. 6b for POPC and other lipids in Fig. S11, the highest total electron density is at z between 16 and 20 Å. The strongest temperature dependence is in the head group and near the terminal methyl group regions, but the hydrocarbon chain region between the head group and tail (10–18 Å) is temperature invariant. In the temperature dependent regions of all PC lipids, the total EDPs indicate that the ED is lower at higher temperature due to expansion of lipid. As the temperature increases, the peaks shift to the left, which is consistent with the reducing bilayer thicknesses.

The simulated component group densities of lipids at 50 °C are shown in Fig. S12. The D_{HH} is estimated based on the total electron density peak distances instead of phosphate group distances [19], because,

Table 4
Hydrocarbon region thickness ($2D_C$) of lipids (Å) at different temperatures.

Lipids	20 °C	30 °C	50 °C	60 °C
DLPC	20.9 (21.9 ± 0.4)	20.9 (21.7 ± 0.4)	21 (20.8 ± 0.4)	20.7 (20.6 ± 0.4)
DMPC	Gel	25.6 (25.7 ± 0.5)	24.9 (24.8 ± 0.5)	24.4 (24.1 ± 0.5)
DPPC	Gel	Gel	28.9 (28.5 ± 0.6)	28.5 (27.9 ± 0.6)
POPC	28.7 (29.2 ± 0.6)	28.1 (28.8 ± 0.6)	28 (28.1 ± 0.6)	27.8 (28.0 ± 0.6)
SOPC	30.7 (30.4 ± 0.6)	29.9 (29.9 ± 0.6)	30.4 (29.3 ± 0.6)	29.6 (29.0 ± 0.6)
DPhPC	27.6 (27.8 ± 0.6)	27.8 (27.2 ± 0.5)	27.7 (26.7 ± 0.5)	27.3 (26.6 ± 0.5)

The data in the first row are MD-based values, and in the second rows with parentheses are the experimental values with uncertainties obtained by Kučerka et al. [19].

even though the total electron density peak is often very close to the electron-dense region of the PC phosphate group, they are not always the same [9]. However, the total electron density peak is overlapping with the electron density of the phosphate group in all lipids within statistical errors in the “peak” determination. Moreover, the carbonyl group is near the interface between the hydrophilic and hydrophobic regions, so it has been used as a quick method to obtain D_C . Here, we provide the comparison between the D_C obtained from carbonyl group distance and that from the volume probabilities (i.e., half of the distance between the midpoints of bilayer’s hydrocarbon acyl chains’ volume probabilities) in different lipids. Fig. S12 shows that DPhPC has smallest distance between D_C and the carbonyl group electron density peak, and DMPC has the largest distance. The carbonyl location is consistently farther away from the center of the bilayer and estimates of the D_C based on carbonyl group electron density peak will be higher than that based on the chain volume. However, this error is rather small as the distance between the D_C location and carbonyl maximal density is 0.45–1.05 Å.

3.4. Deuterium order parameter S_{CD}

Order parameter S_{CD} calculated based on Eq. (2) is compared to available experimental S_{CD} of DLPC, DMPC, and DPPC obtained by Douliez et al. [41] and POPC by Seelig et al. [42].^a The comparison plots of DMPC are shown in Fig. 7. The remaining comparison of DLPC, DPPC, and POPC, as well as the temperature dependence of the S_{CD} of all six lipids are shown in Figs. S13–18. The S_{CD} of each carbon is related to the conformational ensemble average and can be interpreted as a measure of the overall order of bilayer lipids, i.e., a higher value indicates more order in the chain. As the temperature decreases, S_{CD} of almost all carbons increases, therefore the degree of order of the lipid increases, which is consistent with the increase in the bilayer thickness. Compared to the fully saturated PC lipids, unsaturated PC lipids are less linear and the overall bilayer is less ordered (lower S_{CD}). By comparing the S_{CD} of DPhPC to DPPC, the branches decrease the S_{CD} of the attached and neighbor carbons, specially the carbons following the branched carbons.

The MD-based and NMR S_{CD} [41] of DLPC (Fig. S13c) and DPPC (Fig. S15c) match very well at low temperature, while the MD-based S_{CD} is slightly higher than the NMR S_{CD} at higher temperature. For DMPC, the MD-based S_{CD} is slightly greater than the NMR experiments for temperatures at 30, 50, and 60 °C (Fig. 7). For DLPC, DMPC, and DPPC (Figs. S13–15), the C36 MD simulation always gives maximum S_{CD} at C5, while the NMR S_{CD} is nearly constant for C3–C7. The flat values are the consequence of a single signal for these carbons from NMR, which is due to the inability of the experiment to detect the minor variations among them [41]. For POPC (Fig. S16), the MD-based S_{CD} of C12 match NMR S_{CD} [42] very well, but substantial deviation exists at the double bonded C9.

The *sn*-1 chain of POPC and SOPC at 10 °C, and *sn*-2 DMPC at 30 °C show relatively higher S_{CD} than the other temperatures, and more elevated S_{CD} are observed in SOPC in *sn*-2. All these higher S_{CD} may arise from the fact that the simulation temperature is close to their gel-transition temperature: 23 °C for DMPC, −2 °C for POPC, and 6 °C for SOPC. These results suggest that DMPC at 30 °C, POPC at 10 °C, and SOPC at 10 °C may be close to the L_α/L_β phase transition. As shown in Fig. 7, the MD-based S_{CD} at 30 °C are almost identical to the NMR S_{CD} at its gel transition temperature of 23 °C. This result also demonstrates a possibility that the gel-transition temperature DMPC may be slightly higher than 23 °C in the C36 FF. This is likely similar to the other transition temperatures of POPC and SOPC with the C36 FF.

^a We would like to make a correction that reference [42] is also the proper source reference for POPC S_{CD} data used in a previously published paper (reference [14]).

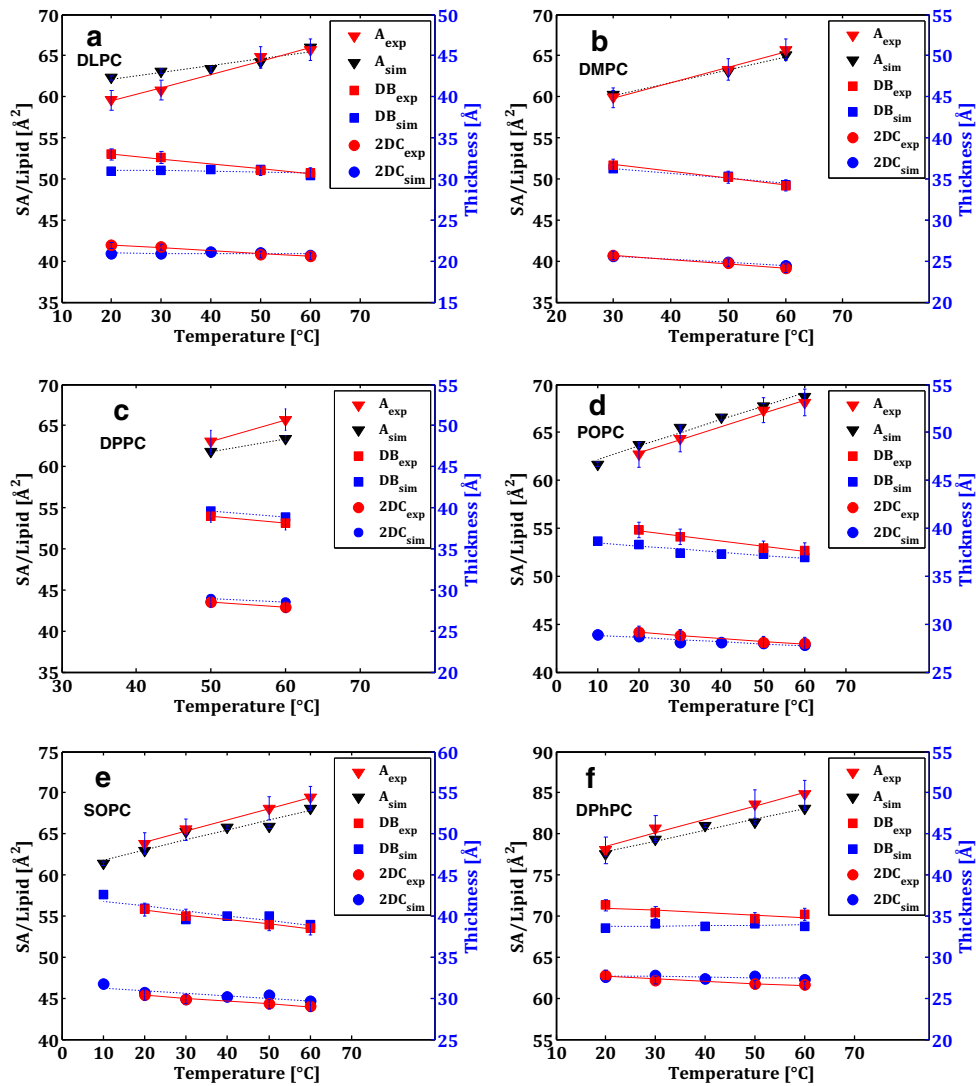


Fig. 5. Comparisons of the SA/lipid and thicknesses (D_B and $2D_C$) from our simulation with Kučerka et al.'s experimentally-estimated data [19]: a) DLPC, b) DMPC, c) DPPC, d) POPC, e) SOPC, and f) DPhPC. Error bars show the uncertainty of experimental values.

3.5. Discussion on discrepancies between experiment and MD simulations with C36 FF

The previous experimental data and the simulation results from a united atom FF 43A1-S3 [52] indicate that $(D_B - D_{HH}) / 2$ or ΔD_{B-HH} remains constant in the range of 0.5 – 1.2 Å at varied SA/lipid [54],

which makes ΔD_{B-HH} to be another important quantity to verify the performance of a lipid FF. However, as shown in Fig. 8, C36 MD-based data show that as the SA/lipid increases, ΔD_{B-HH} decreases. Besides the discrepancy in the SA/lipid dependence, MD simulations with the C36 FF result in smaller ΔD_{B-HH} compared to experimental values. However, based on the ΔD_{B-HH} experimental values of all PC lipids

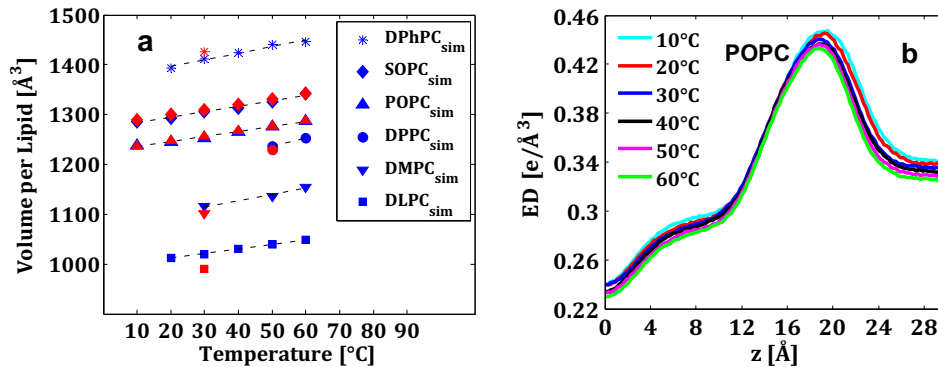


Fig. 6. a) Volume per lipid from the C36 simulations (blue) and the experiments (red) [11,13,40,48]. The experimental V_l of POPC and SOPC are based on the linear fitted parameter to the experimental specific volume data [48]. b) Total electron density of POPC after averaging positive and negative z values at different temperatures.

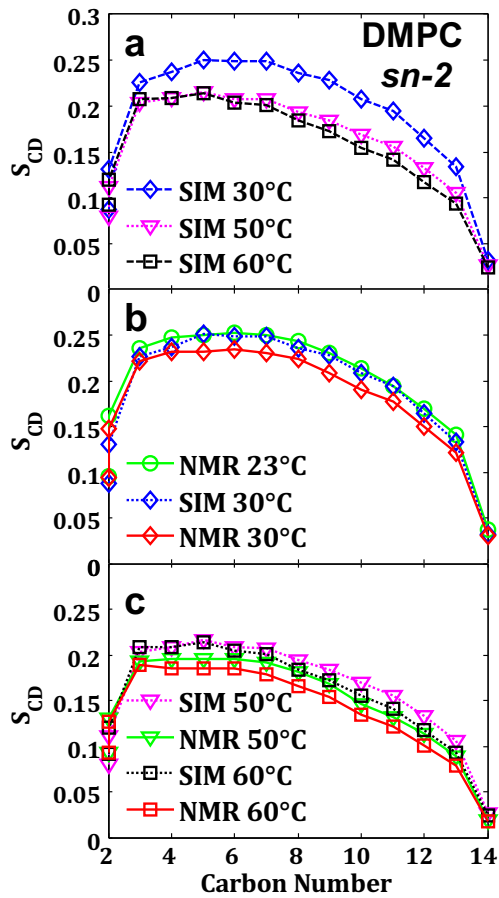


Fig. 7. a) DMPC S_{CD} of *sn*-2 chain at different temperatures. Comparison of MD-based S_{CD} to Douliez et al.'s experimental data [41] at temperatures b) 30 °C, c) 50 °C, and 60 °C. Standard errors for S_{CD} are smaller than the symbol size, so the error bars are not shown.

previously studied, the proposed constant trend and the overall high value of ΔD_{B-HH} in reference [54] appear not to be the case. As shown in Fig. 8, we re-collected the experimental ΔD_{B-HH} of DLPC, DMPC [11], DPPC [13], and DOPC [13,39,43], and also include additional experimental data for POPC [39], DPhPC [40], and SDPC [44]. Fig. S19 demonstrates the data points that John Nagle used [54] and the ones that we added by including more previous experimental data and more lipids that cause the slope change. The decreasing trend is observed in the experimental data with a slope of -0.056 . The C36 MD-based ΔD_{B-HH} shows a similar SA/lipid dependence with a slope of -0.092 .

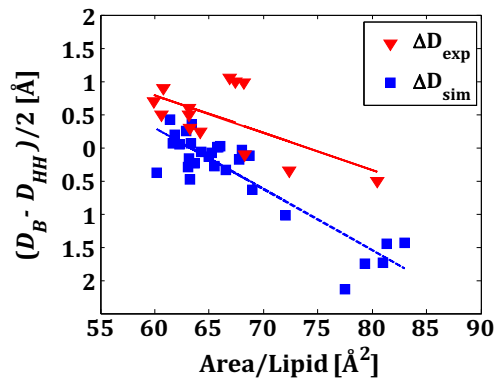


Fig. 8. Comparison of C36 MD-based $(D_B - D_{HH}) / 2$ to experimental values [11,13,39,40,43,44] as a function of the SA/lipid. The slopes of the fitted lines are -0.092 ± 0.009 (simulation) and -0.056 ± 0.021 (experiment).

D_B and D_{HH} strongly depend on the amount of water molecules located in the head group region. For the same temperature, as the SA/lipid increase, the bilayer is more loosely packed. Therefore, more water molecules are located near the polar head groups inside the bilayer, which makes both D_B and D_{HH} smaller. However, since D_B is directly determined by the center of water electron density while D_{HH} is affected by water as well as the electron dense head group components, D_B would decrease more than D_{HH} . Therefore, ΔD_{B-HH} decrease as the SA/lipid increases. Moreover, whether D_B or D_{HH} is greater than each other depends on the SA/lipid and bilayer internal hydration level. There is no reason that ΔD_{B-HH} should remain positive in all circumstances, which is supported by the fact that the experimental ΔD_{B-HH} for POPC is -0.1 \AA [39] and for DPhPC is -0.5 \AA [40]. It is worth noting that except DPPC (at 50 °C), the SA/lipid and the experimental ΔD_{B-HH} values of PC lipids shown in Fig. 8 are measured at 30 °C. Therefore, their difference is mainly caused by intrinsic structural differences of different lipids and also the different analysis method, while the trend of MD-based ΔD_{B-HH} values includes both lipid structural differences and the temperature effect.

There are a few reasons for the discrepancy between the C36 MD-based and experimental form factors and ΔD_{B-HH} . Experimental errors may be one possibility. The ULV sample used in reference [19] are obtained by an extrusion method, in which phospholipid multilamellar vesicles (MLVs) are freeze-thawed and then extruded through filters under high pressure until the vesicles become unilamellar [55]. This method may result in the same issue as in the preparation of the partially-hydrated bilayer crystalline sample, because the pressure applied for extrusion could slightly distort the shape of the ULVs [9]. Such possible distortion of curved LUVs may not be as easy to detect as in the flat bilayer.

Besides the potential experimental errors, the discrepancy could arise from the C36 FF. As mentioned in Section 3.1, MD simulations with the C36 FF agree well with XFF at 30 °C. However, its accuracy decreases as the temperature increases, especially for the second lobe (Figs. 3 and S1–5). We hypothesized that the difference of the form factors and possibly the ΔD_{B-HH} values may be caused by inaccurate density of water and hydrocarbon acyl chains at relatively high temperatures. Therefore, we simulated pure water and heptane systems to trace the temperature dependence of water and heptane density. The comparisons between the MD-based and experimental densities of water [45] and heptane [46] are shown in Fig. 9 and Table S7. At 40 °C, the MD-based density of water is almost same as the experimental values, while at lower temperatures (20 and 30 °C), the MD-based density is slightly higher than experimental values, while it is slightly lower at higher temperatures (50 °C and 60 °C). The density of heptane in MD simulation is smaller than experimental values at all temperatures. Moreover, the density of heptane also decreases faster than experimental data. The consistent accurate representation of the second lobe at 30 °C (which comes from the lipid and water [45,46]) is likely due to cancelation of errors with the water density being slightly high and the hydrocarbon density being consistently low. As the temperature increases, the deteriorated agreement for the second lobe is the result of the combined inaccuracy of the water model and hydrocarbon density.

Since we believe that the water model is the cause of the deviation of the structural parameters, instead of using TIP3P, other water models have the potential to improve the accuracy of the simulation effectively, such as TIP4P/2005 [56]. However, this would require a re-parameterization of the additive CHARMM force field. Another possible reason for these small inaccuracies is that accurate models for water and its interaction with the PC head group require polarizable FFs. C36 is a pairwise additive FF, in which molecules are assigned to fixed charges based on the mean induced dipole in the liquid phase. The dipole moments of water molecules varied greatly in the environment of bulk water and inside the PC lipid head group, even the induced polarization of hydrocarbon tails can affect the dipole

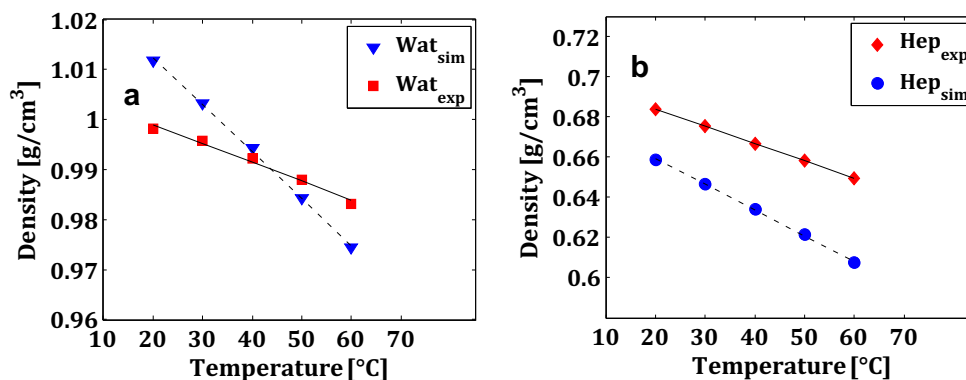


Fig. 9. Comparison of MD-based density of a) water and b) heptane to experimental values [45,46] at different temperatures. The slopes for water are -0.00095 ± 0.00002 (simulation) and -0.00038 ± 0.00003 (experiment) and those for heptane are -0.00128 ± 0.00002 (simulation) and -0.00086 ± 0.000004 (experiment).

potential at the membrane–water interface [57]. However, these are not distinguished in the pairwise additive C36 FF. Therefore, as proposed by Chowdhary et al. [58], the polarizable FF may show better accuracy in the lipid membrane system and improve the agreement with experiment. However, the temperature dependence of the overall density disagrees with experiment for polarizable SWM4-NDP and SWM6 outside 300 K [59,60]. Therefore, we propose that including polarizability might improve water hydration but will likely require improvement beyond that of the Drude water models available in CHARMM.

More importantly, the experimental component density distribution strongly depends on the structural model fits to XFF and NFF [51–53]. The SA/lipid as well as D_B , D_C , and D_{HH} are estimated based on the SDP model applied. Therefore, the model-based experimental value of ΔD_{B-HH} does not provide a reliable tool to justify the accuracy of C36 FF since these data are directly affected by the experimentally-based model(s). The focus should be on the direct comparison between MD simulations and the experimental measures, such as XFF, NFF, NMR, and V_L . It is clear from this work that MD simulations with the C36 FF agree well with the raw X-ray/neutron scattering data, the S_{CD} from NMR experiments, and the experimental V_L .

4. Conclusions

Scattering form factors and S_{CD} calculated from MD simulations with the C36 FF over a range of temperatures match experimental data well, which further proves the general validity of the C36 lipid FF. The MD-based SA/lipid, D_B , D_C , and V_L also show good agreement with model-based experimental values. Both the simulation and experimental data show very similar temperature dependence of structure parameters. As the temperature increases, the SA/lipid and V_L increase, while the bilayer thicknesses and the S_{CD} decrease. Our MD simulations of neat water and heptane suggest that inaccuracies in the water and heptane densities with the C36 FF might be partially a cause for the slight discrepancies between simulation and experiment. Overall, the C36 FF is well suited for studies of L_α bilayers at varying temperatures and is likely appropriate for studies of liquid disordered (L_d) membranes at varying temperatures as seen in biology.

Acknowledgements

This research was supported in part by the following NSF grants MCB-1149187 and DBI-1145652 to (JBK) and ABI-1145987 to (WI). The simulation work was done on the HPCC of DeepThought at the University of Maryland. We would like to thank Josh Nichols for his simulations of DMPC as part of his research project in the Science and Technology (S/T) program at the Eleanor Roosevelt High School in Greenbelt, MD. We specially thank Norbert Kučerka for sharing the

valuable X-ray and neutron scattering data and also SIMtoEXP software for simplifying the data comparison.

Appendix A. Supplementary data

Supplementary data to this article can be found online at <http://dx.doi.org/10.1016/j.bbamem.2014.06.010>.

References

- [1] D.L. Nelson, A.L. Lehninger, M.M. Cox, *Lehninger Principles of Biochemistry*, W. H. Freeman, 2008.
- [2] P.L. Yeagle, Lipid regulation of cell–membrane structure and function, *FASEB J.* 3 (7) (1989) 1833–1842.
- [3] E. Fahy, A comprehensive classification system for lipids (vol 46, pg 839, 2005), *J. Lipid Res.* 51 (6) (2010) 1618.
- [4] L.S. Vermeer, et al., Acyl chain order parameter profiles in phospholipid bilayers: computation from molecular dynamics simulations and comparison with ^2H NMR experiments, *Eur. Biophys. J. Biophys. Lett.* 36 (8) (2007) 919–931.
- [5] J.E. Allen, H. Rasmussen, Human red blood cells – prostaglandin-E2, epinephrine, and isoproterenol alter deformability, *Science* 174 (4008) (1971) 512–514.
- [6] P.G. Kury, P.W. Ramwell, H.M. McConnell, The effect of prostaglandins E1 and E2 on the human erythrocyte as monitored by spin labels, *Biochem. Biophys. Res. Commun.* 56 (2) (1974) 478–483.
- [7] M.J. Ueda, et al., A correlation between membrane fluidity and the critical temperature for cell adhesion, *J. Cell Biol.* 71 (2) (1976) 670–674.
- [8] P.J. Goodford, The effect of temperature changes on the cell membrane, *Ann. R. Coll. Surg. Engl.* 48 (2) (1971) 70–71.
- [9] P. Yeagle, *The Membranes of Cells*, Academic Press, 1993.
- [10] J.F. Nagle, S. Tristram-Nagle, Structure of lipid bilayers, *Biochim. Biophys. Acta Rev. Biomembr.* 1469 (3) (2000) 159–195.
- [11] N. Kucerka, et al., Structure of fully hydrated fluid phase DMPC and DLPC lipid bilayers using X-ray scattering from oriented multilamellar arrays and from unilamellar vesicles, *Biophys. J.* 88 (4) (2005) 2626–2637.
- [12] N. Kucerka, et al., Influence of cholesterol on the bilayer properties of monounsaturated phosphatidylcholine unilamellar vesicles, *Eur. Phys. J. E: Soft Matter* 23 (3) (2007) 247–254.
- [13] N. Kucerka, et al., Lipid bilayer structure determined by the simultaneous analysis of neutron and X-ray scattering data, *Biophys. J.* 95 (5) (2008) 2356–2367.
- [14] J.B. Klauda, et al., Update of the CHARMM all-atom additive force field for lipids: validation on six lipid types, *J. Phys. Chem. B* 114 (23) (2010) 7830–7843.
- [15] J.B. Lim, J.B. Klauda, Branching at the iso- and anteiso-positions in complex chlamydia membranes: a molecular dynamics study, *Biochim. Biophys. Acta Biomembr.* 1808 (1) (2011) 323–331.
- [16] J.B. Lim, B. Rogaski, J.B. Klauda, Update of the cholesterol force field parameters in CHARMM, *J. Phys. Chem. B* 116 (1) (2012) 203–210.
- [17] B. Rogaski, J.B. Klauda, Membrane-binding mechanism of a peripheral membrane protein through microsecond molecular dynamics simulations, *J. Mol. Biol.* 423 (5) (2012) 847–861.
- [18] X. Cheng, et al., CHARMM-GUI micelle builder for pure/mixed micelle and protein/micelle complex systems, *J. Chem. Inf. Model.* 53 (8) (2013) 2171–2180.
- [19] N. Kucerka, M.P. Nieh, J. Katsaras, Fluid phase lipid areas and bilayer thicknesses of commonly used phosphatidylcholines as a function of temperature, *Biochim. Biophys. Acta Biomembr.* 1808 (11) (2011) 2761–2771.
- [20] S. Jo, et al., CHARMM-GUI membrane builder for mixed bilayers and its application to yeast membranes, *Biophys. J.* 97 (1) (2009) 50–58.
- [21] Jo S. Fau – Kim, T., et al., CHARMM-GUI: a web-based graphical user interface for CHARMM. (1096–987X (Electronic)).
- [22] S. Jo, T. Kim, W. Im, Automated builder and database of protein/membrane complexes for molecular dynamics simulations, *PLoS ONE* 2 (9) (2007).

- [23] S.R. Durell, B.R. Brooks, A. Bennaïm, Solvent-induced forces between two hydrophilic groups, *J. Phys. Chem.* 98 (8) (1994) 2198–2202.
- [24] W.L. Jorgensen, et al., Comparison of simple potential functions for simulating liquid water, *J. Chem. Phys.* 79 (2) (1983) 926–935.
- [25] P.J. Steinbach, B.R. Brooks, New spherical-cutoff methods for long-range forces in macromolecular simulation, *J. Comput. Chem.* 15 (7) (1994) 667–683.
- [26] H.C. Andersen, RATTLE — a velocity version of the shake algorithm for molecular-dynamics calculations, *J. Comput. Phys.* 52 (1) (1983) 24–34.
- [27] T. Darden, D. York, L. Pedersen, Particle Mesh Ewald — an NLog(N) method for Ewald sums in large systems, *J. Chem. Phys.* 98 (12) (1993) 10089–10092.
- [28] J.C. Phillips, et al., Scalable molecular dynamics with NAMD, *J. Comput. Chem.* 26 (16) (2005) 1781–1802.
- [29] S. Jo, T. Kim, W. Im, Automated builder and database of protein/membrane complexes for molecular dynamics simulations, *PLoS ONE* 2 (9) (2007) e880.
- [30] S.E. Feller, et al., Constant pressure molecular dynamics simulation: the Langevin piston method, *J. Chem. Phys.* 103 (11) (1995) 4613–4621.
- [31] G.J. Martyna, D.J. Tobias, M.L. Klein, Constant pressure molecular dynamics algorithms, *J. Chem. Phys.* 101 (5) (1994) 4177–4189.
- [32] W. Humphrey, A. Dalke, K. Schulten, VMD: visual molecular dynamics, *J. Mol. Graph.* 14 (1) (1996) 33–38.
- [33] L. Martínez, et al., PACKMOL: a package for building initial configurations for molecular dynamics simulations, *J. Comput. Chem.* 30 (13) (2009) 2157–2164.
- [34] B.R. Brooks, et al., CHARMM: the biomolecular simulation program, *J. Comput. Chem.* 30 (10) (2009) 1545–1614.
- [35] N. Kucerka, J. Katsaras, J.F. Nagle, Comparing membrane simulations to scattering experiments: introducing the SIMtoEXP software, *J. Membr. Biol.* 235 (1) (2010) 43–50.
- [36] J.B. Klauda, et al., Simulation-based methods for interpreting X-ray data from lipid bilayers, *Biophys. J.* 90 (8) (2006) 2796–2807.
- [37] J.H. Ipsen, O.G. Mouritsen, M. Bloom, Relationships between lipid–membrane area, hydrophobic thickness, and acyl-chain orientational order — the effects of cholesterol, *Biophys. J.* 57 (3) (1990) 405–412.
- [38] H. Schindler, J. Seelig, Deuterium order parameters in relation to thermodynamic properties of a phospholipid bilayer. Statistical mechanical interpretation, *Biochemistry* 14 (11) (1975) 2283–2287.
- [39] N. Kucerka, S. Tristram-Nagle, J.F. Nagle, Structure of fully hydrated fluid phase lipid bilayers with monounsaturated chains, *J. Membr. Biol.* 208 (3) (2005) 193–202.
- [40] S. Tristram-Nagle, et al., Structure and water permeability of fully hydrated diphytanoyl PC, *Chem. Phys. Lipids* 163 (6) (2010) 630–637.
- [41] J.P. Douliez, A. Leonard, E.J. Dufourc, Restatement of order parameters in biomembranes — calculation of C–C bond order parameters from C–D quadrupolar splittings, *Biophys. J.* 68 (5) (1995) 1727–1739.
- [42] J. Seelig, N. Waespesarcevic, Molecular order in cis and trans unsaturated phospholipid bilayers, *Biochemistry* 17 (16) (1978) 3310–3315.
- [43] N. Kucerka, et al., Areas of monounsaturated diacylphosphatidylcholines, *Biophys. J.* 97 (7) (2009) 1926–1932.
- [44] N.V. Eldho, et al., Polyunsaturated docosahexaenoic vs docosapentaenoic acid — differences in lipid matrix properties from the loss of one double bond, *J. Am. Chem. Soc.* 125 (21) (2003) 6409–6421.
- [45] W. Wagner, A. Pruss, The IAPWS formulation 1995 for the thermodynamic properties of ordinary water substance for general and scientific use, *J. Phys. Chem. Ref. Data* 31 (2) (2002) 387–535.
- [46] R. Span, Multiparameter Equations of State: An Accurate Source of Thermodynamic Property Data, Springer, 2000.
- [47] N. Kucerka, et al., Curvature effect on the structure of phospholipid bilayers, *Langmuir* 23 (3) (2007) 1292–1299.
- [48] B.W. Koenig, K. Gawrisch, Specific volumes of unsaturated phosphatidylcholines in the liquid crystalline lamellar phase, *Biochim. Biophys. Acta Biomembr.* 1715 (1) (2005) 65–70.
- [49] D. Uhríkova, et al., Component volumes of unsaturated phosphatidylcholines in fluid bilayers: a densitometric study, *Chem. Phys. Lipids* 145 (2) (2007) 97–105.
- [50] J.F. Nagle, D.A. Wilkinson, Lecithin bilayers — density-measurements and molecular-interactions, *Biophys. J.* 23 (2) (1978) 159–175.
- [51] N. Kučerka, et al., Lipid bilayer structure determined by the simultaneous analysis of neutron and X-ray scattering data, *Biophys. J.* 95 (5) (2008) 2356–2367.
- [52] A.R. Braun, J.N. Sachs, J.F. Nagle, Comparing simulations of lipid bilayers to scattering data: the GROMOS 43A1-S3 force field, *J. Phys. Chem. B* 117 (17) (2013) 5065–5072.
- [53] S. Lee, et al., CHARMM36 united-atom chain model for lipids and surfactants, *J. Phys. Chem. B* 118 (2) (2014) 547–556.
- [54] J.F. Nagle, Introductory lecture: basic quantities in model biomembranes, *Faraday Discuss.* 161 (2013) 11–29.
- [55] F. Szoka, D. Papahadjopoulos, Procedure for preparation of liposomes with large internal aqueous space and high capture by reverse-phase evaporation, *Proc. Natl. Acad. Sci. U. S. A.* 75 (9) (1978) 4194–4198.
- [56] J.L.F. Abascal, C. Vega, A general purpose model for the condensed phases of water: TIP4P/2005, *J. Chem. Phys.* 123 (23) (2005).
- [57] E. Harder, A.D. MacKerell, B. Roux, Many-body polarization effects and the membrane dipole potential, *J. Am. Chem. Soc.* 131 (8) (2009) 2760–2761.
- [58] J. Chowdhary, et al., A polarizable force field of dipalmitoylphosphatidylcholine based on the classical Drude model for molecular dynamics simulations of lipids, *J. Phys. Chem. B* 117 (31) (2013) 9142–9160.
- [59] G. Lamoureux, A.D. MacKerell, B. Roux, A simple polarizable model of water based on classical Drude oscillators, *J. Chem. Phys.* 119 (10) (2003) 5185–5197.
- [60] W.B. Yu, et al., Six-site polarizable model of water based on the classical Drude oscillator, *J. Chem. Phys.* 138 (3) (2013).